Quantitative approaches for studying cellular structures and organelle morphology in C. elegans

--Manuscript Draft--

Article Type:	Invited Methods Article - JoVE Produced Video
Manuscript Number:	JoVE59978R2
Full Title:	Quantitative approaches for studying cellular structures and organelle morphology in C. elegans
Keywords:	Quantitative measurements, imaging, Caenorhabditis elegans, synaptic morphology, body wall muscle, myosin length, mitochondrial morphology, Charcot-Marie-Tooth disease
Corresponding Author:	Brent Neumann Monash University Clayton, Victoria AUSTRALIA
Corresponding Author's Institution:	Monash University
Corresponding Author E-Mail:	brent.neumann@monash.edu
Order of Authors:	Jean-Sébastien Teoh
	Ming S Soh
	Joseph J Byrne
	Brent Neumann
Additional Information:	
Question	Response
Please indicate whether this article will be Standard Access or Open Access.	Standard Access (US$2,400)
Please indicate the **city, state/province, and country** where this article will be **filmed**. Please do not use abbreviations.	Melbourne, Victoria, Australia

1 **TITLE:**
2 Quantitative Approaches for Studying Cellular Structures and Organelle Morphology in
3 *Caenorhabditis elegans*
4
5 **AUTHORS AND AFFILIATIONS:**
6 Jean-Sébastien Teoh[1]*, Ming S. Soh[1]*, Joseph J. Byrne[1]*, Brent Neumann[1]
7 [1]Neuroscience Program, Monash Biomedicine Discovery Institute and Department of
8 Anatomy and Developmental Biology, Monash University, Melbourne, Australia
9 *These authors contributed equally.
10
11 **Corresponding author:**
12 Brent Neumann (brent.neumann@monash.edu)
13
14 **KEYWORDS:**
15 *Caenorhabditis elegans*, quantitative measurements, imaging, synaptic morphology, body
16 wall muscle, myosin length, mitochondrial morphology, Charcot-Marie-Tooth disease
17
18 **SUMMARY:**
19 This study outlines quantitative measurements of synaptic size and localization, muscle
20 morphology, and mitochondrial shape in *C. elegans* using freely available image processing
21 tools. This approach allows future studies in *C. elegans* to quantitatively compare the extent
22 of tissue and organelle structural changes as a result of genetic mutations.
23
24 **ABSTRACT:**
25 Defining the cellular mechanisms underlying disease is essential for the development of novel
26 therapeutics. A strategy frequently used to unravel these mechanisms is to introduce
27 mutations in candidate genes and qualitatively describe changes in the morphology of tissues
28 and cellular organelles. However, qualitative descriptions may not capture subtle phenotypic
29 differences, might misrepresent phenotypic variations across individuals in a population, and
30 are frequently assessed subjectively. Here, quantitative approaches are described to study
31 the morphology of tissues and organelles in the nematode *Caenorhabditis elegans* using laser
32 scanning confocal microscopy combined with commercially available bio-image processing
33 software. A quantitative analysis of phenotypes affecting synapse integrity (size and
34 integrated fluorescence levels), muscle development (muscle cell size and myosin filament
35 length), and mitochondrial morphology (circularity and size) was performed to understand
36 the effects of genetic mutations on these cellular structures. These quantitative approaches
37 are not limited to the applications described here, as they could readily be used to
38 quantitatively assess the morphology of other tissues and organelles in the nematode, as well
39 as in other model organisms.
40
41 **INTRODUCTION:**
42 The nematode *Caenorhabditis elegans (C. elegans)* is increasingly utilized as a model system
43 to uncover the biological and molecular processes involved in human disease. An adult
44 nematode has a body length of just over 1 mm, and can produce a large brood of up to 300
45 eggs[1]. After hatching, *C. elegans* only require 3-4 days to reach adulthood, and live for around
46 2 to 3 weeks[2]. Due to its ease of culturing, *C. elegans* is currently one of the most sought-after
47 in vivo animal models for conducting cost-effective, rapid drug screening to identify

therapeutics for human diseases. Additionally, its genetic conservation, well defined behavioral paradigms, transparent body for fluorescence or light microscopy, and ease of genetic manipulation make the study of cellular and molecular consequences of genetic mutations readily achieveable[3]. The *C. elegans* genome shares approximately 60-80% orthology with human genes, and about 40% of those genes are known to be disease-related. Some of human diseases that have been modelled and studied in *C. elegans* include neurodegenerative disorders (Alzheimer's disease, Parkinson's disease, amyotrophic lateral sclerosis, Charcot-Marie-Tooth disease), muscle-associated diseases (Duchenne muscular dystrophy), and metabolic diseases (hyperglycemia)[2,4]. In most human disorders, disease-induced cellular and organelle localization and morphological changes occur, which can readily be evaluated in the nematode model.

Fluorescent markers have been widely used to label tissues and organelles for dynamic visualization under the microscope. However, in *C. elegans*, conventional methods that assess morphological irregularities due to genetic mutations have largely relied on visual descriptions. While qualitative assessments can cover wider ranges of phenotypic descriptions (synaptic morphology, GFP clumping, specific axonal shape, muscle fiber thickness, etc.) and provide a bird's eye view of the morphological changes, they are less well suited for comparing small variations across different groups. Furthermore, qualitative assessments are based on visual, subjective evaluation, which may lead to over- or under-estimations of morphological abnormalities. Finally, qualitative observations can also vary greatly between individuals, creating difficulties with data replication.

In recent years, a number of user-friendly, readily available computational algorithms that can quantitatively analyse images have been developed. However, the utilization of such image analysis software for some morphological studies, especially in relation to body wall muscles and mitochondria, in *C. elegans* research has lagged behind. To improve underlying structural analysis in *C. elegans*, some of the readily available, open-source image analysis software were trialed to quantitatively compare the effects of genetic mutations on muscle mitochondria, body wall muscle and synaptic morphology. These experimental procedures outline in detail how these programs (Fiji, ilastik, CellProfiler, SQUASSH) can be used to evaluate changes in synaptic size and synaptic protein localization, body wall muscle area and fiber length, and mitochondrial size and circularity as a result of genetic mutations in the nematode.

PROTOCOL:

1.   Growth and maintenance of *C. elegans* strains

1.1.   Seed Nematode Growth Medium (NGM, see **Table of Materials**) agar plates with 300 µL of the slow-growing *E. coli* strain OP50 in a laminar flow cabinet.

1.2.   Leave the NGM agar plates in the laminar flow cabinet to dry.

NOTE: In the absence of laminar flow cabinet, plates can be left to dry on the bench but they are more prone to contamination.

95   1.3.   Transfer at least 20 animals to each of two OP50-seeded NGM agar plates to have
96   working stocks. There are two main ways to transfer animals.
97
98   1.3.1. Picking: Gently lift the animals using a heat-sterilized pick. This method is effective for
99   selecting individual or multiple animals from an agar plate. Having a small scrape of bacteria
100   at the tip when picking helps the transfer.
101
102   NOTE: A pick is made of a small piece of platinum wire about 4 cm long that is embedded in
103   a glass pipette, with the wire tip flattened to be 'spear-like'. Heat-sterilize the pick between
104   picking to prevent cross-contamination.
105
106   1.3.2. Chunking: Using a sterilized spatula, cut a small square of agar containing the animals
107   from one plate and transferred upside-down to a new plate.
108
109   NOTES: This method is generally useful for transferring large numbers of worms, and to
110   remove contamination from plates through multiple rounds of chunking non-contaminated
111   agar. Avoid cross-contamination by flaming the spatula for a few seconds and immersing the
112   spatula in 100% ethanol between transfers. Transferring from starved plates is not
113   recommended as starvation and overcrowding can affect the health and morphology of
114   cellular and subcellular structures.
115
116   1.4.   Maintain the worms at standard growth temperature (20 °C). To ensure continuous
117   supply of well-fed worms, transfer the worms to new OP50-seeded plates every 2 to 3 days.
118
119   **2.   Age-synchronizing *C. elegans***
120
121   2.1.   Maintain the worms on 3-4 NGM plates until the population is crowded but not
122   starved.
123
124   2.2.   Gently wash the worms off the NGM plate with M9 solution. The eggs will remain on
125   the plate since they stick to the *E. coli OP50*. Repeat with four additional wash steps to remove
126   all hatched animals.
127
128   2.3.   Allow the worms to hatch for 40 min.
129
130   2.4.   Add 1-2 mL of M9 solution to the plate and gently swirl to loosen recently hatched
131   worms.
132
133   2.5.   Collect the M9 solution with recently born worms and transfer the solution with
134   worms to a fresh NGM plate.
135
136   2.6.   Allow the M9 solution to evaporate by exposing the NGM plate to air. Do this adjacent
137   to an open flame to avoid contamination of the NGM plate.
138
139   2.7.   Grow the worms for 27 h at 20 °C to allow development into the third larval (L3) stage.
140   For synchronized 3-day old adult animals, the worms are picked at larval stage 4, and grown
141   for a further 3 days to reach 3-day old adult stage.

**3.	Preparation of slides for imaging**

3.1.	Prepare 3-4% w/v agarose stock in a microwave-safe bottle (3-4 g in 100 mL of ultrapure water).

NOTE: Agar can be used in place of agarose at the same concentration.

3.2.	Melt the agarose carefully in a microwave oven, taking care not to over boil, until all agarose dissolves (clear solution). Keep the solution at 70 °C to prevent solidification.

NOTE: Agarose stock can be used several times. Reheat before use if the agarose has solidified.

3.3.	Using a Pasteur pipette, place a drop of melted agarose onto a microscope slide.

NOTE: Avoid having air bubbles in the drop of agar as these disrupt the integrity of the pad.

3.4.	Immediately press down the agarose droplet with another microscope slide, gently flattening the agarose into a pad between the two slides.

NOTE: Any leftover bubbles should be removed at this stage. If not, new slides should be made as animals can easily get stuck in the bubbles. Avoid overflow of agar to the side when pressing on the slide.

3.5.	Leave the agarose to dry for 1 min.

3.6.	Carefully separate the two slides to avoid damage to the agarose, while leaving the solidified pad on one of the slides.

NOTE: Slides with agarose pads should always be prepared fresh just before the experiment as they can dry out. Make sure the agarose pad has a consistent thickness. There should be no air bubbles or cracks in the pad as this may interfere with imaging.

3.7.	Add a small drop (5-10 μL) of 0.05% tetramisole hydrochloride (anesthetic) to the center of the agarose pad.

3.8.	Using heat-sterilized pick, quickly transfer about 10 – 15 animals from the stock plate to the anesthetic droplet before the solution dries out. Avoid transferring too much OP50 bacteria as this makes the solution cloudy, which can interfere with imaging.

NOTE: If the anesthetic solution dries out while picking, simply pipette a second drop of 0.05% tetramisole hydrochloride onto the animals. The animals tend to lay on their lateral side in the anesthetic solution.

187 3.9.   Apply a coverslip by positioning it just above the agarose pad and gently dropping it
188 down. This will prevent the formation of bubbles. Do not apply pressure to the coverslip as
189 this may crush the animals.
190
191 3.10.   Label the slides with the strain name.
192
193 **4.   Assessing synaptic morphology**
194
195 NOTE: The effects of MEC-17 overexpression on synapse integrity in the posterior lateral
196 microtubule (PLM) touch receptor neurons were studied by quantifying the synaptic size and
197 localization using line scanning confocal microscopy. The PLM neurons (including the synaptic
198 regions) were visualized using the *uIs115(Pmec-17::tagRFP)* transgene (strain: TU4065[5]) and
199 the synaptic region was specifically labeled with *jsIs37(Pmec-7::snb-1::GFP)* (strain: NM664[6]).
200 This study was performed in synchronized L3 non-transgenic and transgenic animals of the
201 extrachromosomal MEC-17 overexpression strain BXN507 [*cjnEx036(Pmec-4::mec-17, Pmyo-*
202 *2::mCherry); jsIs37; uIs115*][7]. A complete list of strains used in this study is included in **Table**
203 **1**.
204
205 4.1.   Confocal imaging of touch receptor neuron synapses
206
207 4.1.1.   To image the synaptic regions, use a line scanning confocal microscope coupled to a
208 488 nm and 552 nm optically pumped semi-conductor diode laser and equipped with image
209 capture software.
210
211 4.1.2.   Locate the worms using the lowest magnification.
212
213 4.1.3.   When the animals are successfully situated, switch to a 40X magnification and apply
214 immersion medium (in this study: a 40X/1.10 HC PL APO CS2 multi-immersive objective with
215 water immersion was used).
216
217 4.1.4.   Visualize the synaptic region by exciting the fluorophores with a 488 nm laser (2%
218 power) for the GFP fluorophore and 552 nm (1% power) for the tagRFP fluorophore.
219
220 4.1.5.   Determine optimal x and y frame to capture the entire synaptic region. Make sure to
221 consider the optimal pixel size when selecting the frame. In this study, a consistent pixel size
222 of 56 nm was obtained.
223
224 4.1.6. Capture images using a hybrid photo-detector and set the gains to prevent
225 overexposure of the fluorophores (100% for 488 nm excitation and 15% for 552 nm
226 excitation).
227
228 4.1.7.   Collect z-stack images to cover the entire synapse, using the optimal z-step size
229 depending on the specific objective used. In this study, an optimal z-step size of 0.211 nm was
230 used.
231
232 NOTE: Ensure all images are taken under stringent condition to allow integrated fluorescence
233 quantification and comparison. This can be done by keeping microscopy parameters identical

234 across all captured images (i.e., laser and detector settings, pixel size, scanning speed, and
235 optimal z-step size). Optimal settings depend on the objective and can be calculated using
236 accessible bioinformatics programs, such as the Nyquist calculator
237 (https://svi.nl/NyquistCalculator). Label images systematically, this will be useful when using
238 bioinformatics software that will organize and process files based on filename.
239
240 **4.2.   Quantification of the synaptic region**
241
242 4.2.1. To analyze the synaptic region, export images as TIFF files. Java based imaging
243 processing software such as ImageJ, can be used (in this study, the MRI image conversion
244 macro in ImageJ was used).
245
246 4.2.2. The size and the integrated fluorescence intensity levels of synapses were measured
247 from sum intensity of the obtained z-stacks with CellProfiler-3.1.5. Load the images into the
248 CellProfiler3.1.5 software. If required, images can be filtered based on image filenames.
249
250 4.2.3. Set up the Name and Type module. Optionally, extract the metadata from the image
251 label to organize calculated data accordingly.
252
253 4.2.4. Determine the synaptic region by hand definition of this region using the diffuse
254 tagRFP expressed from the *uIs115(Pmec-17::tagRFP)* transgene. This can be done by adding
255 the regarding module to the CellProfiler-3.1.5 pipeline.
256
257 4.2.5. To measure the size and fluorescence of the hand defined synapse, add the **Measure**
258 **object size and shape** and **Measure object intensity** module to the pipeline.
259
260 4.2.6. Calculate the relative integrated fluorescence intensity by adding the **Calculate Math**
261 module. Divide the integrated intensity units obtained from *jsIs37(Pmec-7::snb-1::GFP)* by the
262 integrated units obtained for *uIs115(Pmec-17::tagRFP).*
263
264 4.2.7. Export measurements and calculations.
265
266 **5.   Quantifying body wall muscle structure**
267
268 5.1.   **Fluorescence** imaging of body wall muscle structure
269
270 5.1.1. Obtain a strain (for example, RW1596) carrying the transgene *stEx30(Pmyo-*
271 *3::gfp::myo-3 + rol-6(su1006))*[8], which labels myosin fibers with GFP.
272
273 NOTE: Introduction of the transgene into animals can be achieved by either crossing a strain
274 of interest with animals that already express the transgene, or microinjecting DNA into the
275 distal arm of the gonad. The 'rolling' phenotype induced by *rol-6* mutation in this transgene
276 facilitates the visualization of the muscles. The body wall muscles run along the dorsal and
277 ventral sides that are normally precluded from view in wild-type animals because they
278 typically lie on one of their lateral sides. The *rol-6(su1006)* allele induces twisting of the
279 animals, thereby exposing some muscles cells for imaging.
280

281 5.1.2. Image the animals using a fluorescence microscope coupled with a high resolution
282 charged coupled device camera (CCD), 40X objective or higher, GFP filter and acquisition
283 software.
284
285 5.1.3. Adjust the exposure time and illumination intensity to prevent oversaturated images.
286
287 5.1.4. Capture and save images of muscles (400X magnification) from a section of the animal
288 containing at least one complete visible oblique muscle cell. Avoid regions with a single
289 muscle cell that is incomplete or sections that are out of focus. Also exclude images from
290 extreme anterior and posterior regions, and regions adjacent to the vulva.
291
292 NOTE: If the animal does not have a single visible complete muscle cell, gently slide the
293 coverslip to turn the animal so as to expose a complete cell.
294
295 **5.2.   Measurement of muscle cell area**
296
297 5.2.1. Open the image in Fiji software[9] (version 2.0.0 was used in this study).
298
299 5.2.2. Use the polygon selection to carefully trace around a single oblique muscle cell. Adjust
300 the line of the polygon at the end by dragging the anchor dot to improve tracing.
301
302 5.2.3. Go to **Analyze** tab at the top of the software and click **Measure** to calculate the area
303 of the selection. A separate results table containing the area and other measurements will be
304 shown. If the area measurement is missing from the results table, go to **Set Measurements**
305 under the **Analyze** tab and check that the area box is ticked. Likewise, untick other
306 measurements that are not needed.
307
308 5.2.4. For muscle cells with a degenerated/missing region, trace the missing region with the
309 polygon selection tool and click **Measure** again. If there are multiple gaps within the cell, trace
310 each gap separately.
311
312 5.2.5. Calculate the ratio of gap area to the entire single muscle cell. A high ratio indicates a
313 higher extent of muscle degeneration due to large gaps within the cell. If there are no missing
314 regions, as commonly seen in wild-type animals, the ratio would be calculated as zero.
315
316 NOTE: As a control, score also for muscle structure defects visually and compare results with
317 the quantitative measurement. This is especially useful if the strain is being studied for the
318 first time in the lab. For phenotypic scoring, assess the animals as defective or not-defective
319 based on the integrity of the filaments. For example, animals with loss of distinct filament
320 striations, GFP clumping, or gaps within muscle cells due to structural breakdown, would be
321 scored as defective.
322
323 **5.3.   Segmentation and quantification of myosin fiber length**
324
325 5.3.1. If necessary, first convert files to *.tif* using Fiji or another software package. Save the
326 TIFF files in desired location.
327

328   5.3.2. Open ilastik[10] (free software, version 1.3.2 can be downloaded from
329   https://www.ilastik.org/).

331   5.3.3. Once in ilastik, choose **Pixel Classification** under **Create New Project**. The software
332   will prompt for the project to be saved. Rename the project and save to a desired location.

334   NOTE: A new project only needs to be created once. Subsequent segmentation can be done
335   using the same project. To use the same project settings, go to **Project** tab at the top, and
336   click on **Open Project** to access the project file.

338   5.3.4. There should be 5 tabs on the left panel (Input Data, Feature Selection, Training,
339   Prediction Export and Batch Processing). In the **Input Data** tab, click on **Add New** and then
340   **Add separate image(s).** Direct the pop-up window to the folder containing the TIFF files and
341   select the image to open.

343   5.3.5. In the next tab below (**Feature Selection**), click on **Select Features** to select all pixel
344   features, indicated by green ticked boxes. The pixel selection in this step is used to distinguish
345   the different classes of pixels in the next step.

347   NOTE: Pixel feature selection depends on the image resolution. Hence, the developers
348   suggest to select all or as many features as possible, if the processing power and time permit.

350   5.3.6. The following **Training** panel allows the classification of different object classes based
351   on pixels. In this case, the two classes are the individual GFP-expressing myosin filaments and
352   unwanted background or blurred edges. Click on **Add Label** to have the first label. Scrawl over
353   a number of filaments to begin classifier training.

355   NOTE: Double-clicking the label allows for name change (for example, renaming 'label 1' to
356   'filament'). Double-clicking the colored box allows colors for drawing and probability displays
357   to be altered. The default size of the paintbrush is 1, although the size can be increased to 61.
358   If the wrong pixel has been drawn, simply use the eraser tool to remove the drawing.
359   Keyboard controls (-) and (Shift +) can be used to zoom in and out of image, respectively.
360   Arrow keys are used to navigate around the image.

362   5.3.7. Add a second label and rename it to **Background**. Scrawl over unwanted backgrounds
363   and spaces between the filaments.

365   5.3.8. Click on **Live Update** and make sure that classification has been done by the software
366   correctly. Add more scrawls and fine tune the training if necessary.

368   NOTE: It is important to keep an eye out for merged fibers and blurry edges (such as body
369   line) in this step. Improve the prediction here as much as possible to increase the accuracy of
370   measurements. The prediction accuracy also depends on image resolution, as pixels in low
371   quality images are more difficult to tease apart. It is also optional but recommended to run
372   the **Filter Method** in the **Suggest Features** function next to **Live Update** control.

374 <mark>5.3.9. Once training classifier has been adequately performed, go to **Prediction Export**</mark>
375 <mark>panel. Click on **Choose Export Image Settings** with **Probabilities** as the source.</mark>

376

377 <mark>5.3.10. Use the following settings. cut-out subregion *x* and *y* ticked, and *c* unticked. The start</mark>
378 <mark>and stop values for *c* should be 0 and 1, respectively. Tick and convert data type in</mark>
379 <mark>**Transformations** to unsigned 8-bit, tick renormalize [min, max] and use the default values.</mark>
380 <mark>Change the format of the output file video to PNG, and rename the file and directory as</mark>
381 <mark>desired.</mark>

382

383 <mark>5.3.11. Close the export settings window and export the specific image that has just been</mark>
384 <mark>segmented.</mark>

385

386 <mark>5.3.12. Open the saved PNG image in Fiji software. The image should appear in black and</mark>
387 <mark>white.</mark>

388

389 <mark>5.3.13. Adjust the threshold of the image using the default settings.</mark>

390

391 <mark>5.3.14. Apply the skeletonization plugin (Skeletonize 2D/3D, and then Analyze Skeleton). A</mark>
392 <mark>separate table of results will be displayed, which includes branch length. The branch length</mark>
393 <mark>represents the fiber length. Other data in the results could also be useful, such as Euclidean</mark>
394 <mark>distance.</mark>

395

396 NOTE: Omit fibers with lengths of 0 μm or more than 250 μm, as these sizes are not
397 physiologically possible.

398

399 **6. Quantifying mitochondrial morphology**

400

401 NOTE: For the quantification of mitochondrial morphology, this study used the BXN038[7] strain
402 containing the *uIs115(Pmec-17::tagRFP)*[5] transgene to visualize the PLM neurons and
403 *jsIs609(Pmec-4::MLS::GFP)*[11] to visualize mitochondria specifically within the PLM neurons.
404 This study was performed in synchronized 3 day old adult worms, but has successfully been
405 performed at other ages, as well as in other tissues[7].

406

407 **6.1.   Fluorescence imaging of mitochondria within the PLM neurons**

408

409 6.1.1. To measure size and shape changes of mitochondria within the PLM neurons, visualize
410 both the background neuron and mitochondria using fluorescent transgenes.

411

412 6.1.2. To image the PLM neuron, use a confocal microscope coupled to a 488 nm and 552
413 nm optically pumped semi-conductor diode laser and equipped with image capture software.

414

415 6.1.3. Image the worm as per steps 4.1.1-4.1.4 above, ensuring non-saturating exposure
416 conditions.

417

418 6.1.4. In order to visualize the entire neuron, a tiled image may be needed. To achieve this,
419 use software with a tile scan option to locate and drop a marker at one corner of the neuron

420 and then locate the opposite end and drop the other marker. The software will calculate the
421 optimal number of tiles needed to capture the required area.

423 NOTE: To reduce scanning time, it is often easier to locate neurons that follow one single
424 plane, resulting in fewer tiles.

426 6.1.5. To couple the tile scan with a Z-stack, set the lower and upper limits prior to starting
427 the tile scan, and ensure that the optimal slice size is set.

429 6.1.6. Ensure resolution is optimized, as segmentation will be more refined with higher
430 resolutions (here, a resolution of 3224 x 3224 pixels was used).

432 NOTE: Whilst the *uIs115(Pmec-17::tagRFP)* transgene is used to mark the PLM and
433 successfully position the camera, it does not necessarily need to be imaged due to slight
434 background fluorescence observed from the *jsIs609(Pmec-4::MLS::GFP)* transgene within the
435 PLM axon itself. Thus, scanning and imaging time can be reduced by removing the 552 nm
436 filter from the experiment.

438 6.2.   Object segmentation using SQUASSH

440 6.2.1. Convert image files into *.tiff* images and generate maximum intensity projections from
441 Z-stacks using Fiji imaging software. Crop images to the minimal size while still containing the
442 complete neuron to reduce computational load and reduce background noise.

444 NOTE: For the representative results, only mitochondria within the long axonal processes
445 were considered, so the cell body and any mitochondria within were excluded from each
446 image.

448 6.2.2. Using the Mosaic Suite SQUASSH macro for ImageJ, perform Split Bregman
449 segmentation[12] on the maximum projections. A detailed guide to the installation and
450 application of this macro is available on the Mosaic website (http://mosaic.mpi-cbg.de/) and
451 described by Rizk et al. 2014[13]. The process of image segmentation is described in short
452 below.

454 NOTE: This segmentation identifies objects (in this case individual mitochondrion) over a
455 threshold of fluorescence intensity, allowing for accurate measurement of each individual
456 objects size and shape.

458 6.2.3. Remove background noise from an image using the rolling ball method, in which a
459 user defined window moves across the image, imputing the local background intensity
460 estimate from the most frequently occurring intensity in each window. This corrects uneven
461 background intensities.

463 6.2.4. Use object detection to roughly find regions of the image that contain objects
464 (mitochondria) of interest, based on the fluorescence intensity and number of pixels. The
465 parameters that govern this step are regularization and minimum object intensity.

466

467   NOTE: Regularization is used to avoid segmenting small intensity, noise-induced peaks, and
468   the minimum object intensity threshold helps to define the subcellular organelles from
469   background tissue fluorescence. These are the main two parameters that are manipulated to
470   find an optimal segmentation of mitochondria, and the optimization process tends to be trial
471   and error of different parameters for a test image, followed by manual inspection.

473   6.2.5. Use the software to estimate the local background intensities around each object to
474   aid computation of optimal segmentation.

476   6.2.6. Measure individual objects for size, perimeter, length via pixel number, as well as
477   signal intensity and x/y location on the image. To calculate measurements in size (nm), factor
478   in the pixel size of the original image.

480   NOTE: For each experiment, optimal parameters must first be calculated. To ensure accuracy
481   of segmentation, it is advisable to perform a SQUASSH analysis on a test image and manually
482   inspect the accuracy of segmentation. The macro provides output files showing the individual
483   objects that were identified on the original image, and inspecting these closely and adjusting
484   parameters to suit will ensure an accurate segmentation. The defined parameters must then
485   be used for the entire experiment for comparability. The parameters used for the
486   representative results are included in **Table 2**.

488   6.2.7. Open Fiji or ImageJ analysis software, navigate to the Mosaic macro container and
489   open the SQUASSH menu.

491   6.2.7.1.   Open the **Background Subtraction** submenu and ensure **Remove background?**
492   is checked. The default for window size is 10.

494   6.2.7.2.   Set the desired **Regularization** and **Minimum object intensity, channel 1**
495   values to best identify and segment objects (see step 6.2.4). **Channel 2** values are not
496   necessary for objects marked with a single transgene.

498   6.2.7.3.   Click the **Estimate PSF from objective properties** to estimate the Point Spread
499   Function based on the microscope's characteristics. This helps the segmentation of closely
500   located objects by accounting for the influence of each pixel on its neighboring pixel.

502   NOTE: **Subpixel segmentation** was not used in this experiment due to its increased load on
503   computer processing power. **Cell masks** were also not used as the axon is easily defined.
504   These settings are useful for more complex tissues and to define objects on a cell by cell basis.

506   6.2.7.4.   For visualization options, ensure **Object outlines** and **Save object and image**
507   **characteristics** are checked. For use later in graphics and statistical software, ensure the
508   correct number of conditions are input.

510   6.2.8. Locate the folder with *.tiff* images and run the macro. This process can be performed
511   on an individual image or on a batch of images per genotype located within a folder. Output
512   files will be located in the folder along with the original images.

513

6.3.   Analysis and measurements of shape

6.3.1. Use the output from SQUASSH to provide an itemized object data *.csv* file, which provides each individual object per row including its measurements as described above.

NOTE: While this macro process automates object measurements, it is always important to manually check output images after SQUASSH segmentation to ensure the macro has properly identified mitochondria.

6.3.2. To analyse the shape of each mitochondria, use a two-dimensional measure for sphericity, **Circularity**, to estimate the deviation of the object from a perfect circle.

NOTE: Circularity is a function of area and perimeter (Circularity = (4 x π) x (Area/Perimeter^2) where 1 = a perfect circle and 0 = a straight line. This can be achieved using a formula in graphics and statistical software.

6.3.3. To determine the variance in size and shape across the pool of mitochondria, calculate histograms and a fitted Gaussian distribution using graphics and statistical software, with bins of 0.2 μm for mitochondrial size and 0.05 for mitochondrial circularity.

REPRESENTATIVE RESULTS:
C. elegans is an ideal model organism for studying morphology of different tissues and organelles due to its simplicity, known cell lineage, transparency, and available tools. Here, we provide quantitative approaches for studying organelles (e.g., mitochondria) and tissues, including synapses and muscles using live fluorescence imaging and free bio-image processing software.

Strict regulation of MEC-17 expression is required for normal synapse development
To further understand the function of the alpha-tubulin acetyl-transferase MEC-17[14-16] in the nervous system, we studied synaptic morphology in the touch receptor neurons in *C. elegans* overexpressing the protein[17]. These cellular structures are essential for neuron function as they allow signals to be passed on to neighboring neurons. Images of the PLM synapse were collected using a laser scanning confocal microscope and quantitative morphology analysis was performed using accessible bio-image processing software (**Figure 1A,B**). The overexpression of MEC-17 results in significant reductions in the area of pre-synaptic accumulations in PLM and reduced relative integrated fluorescence intensities of the SNB-1::GFP marker (**Figure 1C,D***). Together, these results suggest that overexpression of MEC-17 disrupts normal synapse development in the PLM touch receptor neurons.

The size of the presynaptic site and relative integrated fluorescence were studied using the free bio-image processing software CellProfiler3.1.5. Due to their complex structure, synapses were defined by hand using the diffuse tagRFP protein expressed from the *uIs115(Pmec-17::tagRFP)* transgene. The area of the defined synapse was calculated by the number of pixels within the defined region. Compared to the wild-type control, animals overexpressing MEC-17 have significantly reduced pre-synaptic regions (P = 0.0025; n ≥ 10) (**Figure 1C**). In addition, to study synaptic integrity, relative integrated fluorescence intensity levels were compared. This was calculated by measuring integrated fluorescence intensity

561 levels within the defined synapse for both SNB-1::GFP and the diffusible tagRFP.
562 Subsequently, the SNB-1::GFP fluorescence values relative to tagRFP values were compared
563 for which a significant decrease ($P = 0.0479$; n ≥ 10) was observed with the overexpression of
564 MEC-17 (**Figure 1D**). Together, these results suggest that the correct regulation of MEC-17 is
565 important for synapse development.
566
567 **Quantitative measurement of body wall muscle cell area and fiber length reveals significant**
568 **defects as a result of mutations in CMT2-related genes**
569 Mutation in the genes *MFN2*, *DNM2* and *KIF5A* have been shown to cause Charcot-Marie-
570 Tooth type 2 (CMT2), an axonal form of the most common inherited peripheral
571 neuropathy[18,19]. CMT2 is commonly associated with slowly progressive distal muscle
572 weakness and atrophy, distal sensory impairment, foot deformities and secondary steppage
573 gait. As a result, patients often suffer debilitating lifelong mobility impairments. There is
574 currently no cure for the disease, partly due to genetic and clinical heterogeneity associated
575 with CMT2[19], as well as a lack of animal models to study disease pathophysiology. Hence,
576 using animal models to understand the underlying cellular defects can provide answers to the
577 unknown CMT2 disease mechanisms.
578
579 Thus far, published studies evaluating body wall muscle defects in *C. elegans* have relied on
580 visual scoring rather than quantitative measurements[20]. In order to avoid subjective bias that
581 can occur during qualitative assessment, quantitative measurements of body wall muscle
582 area and myosin fiber length were trialed using available image processing programs. We
583 used these methods to assess muscle morphology in animals carrying mutations in the *fzo-*
584 *1/MFN2*, *dyn-1/DNM2* and *unc-116/KIF5A* genes in 3-day old adult *C. elegans*. For both
585 measurements, a number of conditions were applied, such that at least a single complete
586 oblique muscle cell was within view, muscle cells that were fuzzy or out of focus were
587 excluded, and extreme anterior and posterior regions, as well as regions adjacent to the vulva
588 were omitted. In addition to the mutations in the CMT2-associated genes, animals also
589 carried the *stEx30(Pmyo-3::gfp::myo-3 + rol-6(su1006))* transgene that labels a *C. elegans*
590 myosin heavy chain subunit with GFP (**Figure 2A-E**). The simple polygon tool in Fiji software[9]
591 (version 2.0.0) was used to measure the area of a single muscle cell. If an animal experienced
592 body wall muscle structure breakdown, leaving behind empty spaces within muscle cells, the
593 ratio of gap area to total single muscle cell area was calculated and compared to wild-type
594 control (**Figure 3A**). To obtain measurements of myosin fiber length, each image was first
595 segmented using ilastik software[10] (version 1.3.0) (**Figure 3B**). Segmentation is a process that
596 allows the individual muscle fibers to be classified and separated from unwanted sections
597 such as the background. Following segmentation, the image was exported as an unassigned
598 8-bit binary image. Fiji (version 2.0.0) was next used to **Skeletonize** the binary image to filter
599 out border pixels, leaving behind fragments representing the original fibers. The branch
600 lengths of the **Skeletons**, or individual myosin filaments, were then analyzed in Fiji. Length
601 measurements of 0 or more than 250 µm, which is the maximum reasonable length for a
602 filament even with muscle stretching, were excluded. Altogether, between 2000 to 3000
603 myosin fiber lengths were measured. A summary of the segmentation workflow is shown in
604 **Figure 3B**. Results from the quantitative analysis were further compared with visual scoring
605 of body wall muscle defects, where 3-day old animals were categorized as defective or not-
606 defective based on muscle structure integrity.
607

608 Defects in body wall muscle morphology were observed between 2.5 to 3.5 times higher in
609 *fzo-1(cjn020)*, *dyn-1(ky51)* and *unc-116(e2310)* animals than in wild-type animals during
610 visual assessment (**Figure 4A**). Most animals with mutations in *fzo-1* and *unc-116* experienced
611 conspicuous loss of muscle striations, large GFP clumping due to accumulation of cellular
612 debris, and muscle fiber degeneration that left gaping space within muscle cells (**Figure 2C,E**).
613 In contrast, while more than 60% of *dyn-1* mutants were scored visually defective, the extent
614 of defects was minimal compared to the other two genetic mutants. There was only slight
615 loss of striations, no GFP aggregations and only minor muscle degeneration when compared
616 to the other two mutants (**Figure 2D** and **Figure 4A**). As with other phenotypic scoring, the
617 extent of the defects could not be considered, and a tendency for bias might cause a higher
618 proportion of defects to be registered. Therefore, quantitative measurements of muscle cell
619 area and fiber length would provide a more accurate representation of the extent of muscle
620 defects than visual assessment alone. In line with the large gaps observed with visual scoring,
621 the ratio of gap area to total single cell area was shown to be 5 to 6 times higher in *fzo-1* and
622 *unc-116* mutant animals compared to the wild-type group, which only experienced negligible
623 muscle structure breakdown (**Figure 4B**). The lack of structural collapse in *dyn-1* mutants
624 resulted in a non-significant, 3-fold increase in gap to muscle cell area ratio (**Figure 4B**). This
625 also indicates that experimenter bias might be a factor contributing to the high proportion of
626 defects assigned by qualitative assessment. Nevertheless, the small gaps decreased the
627 average fiber length from 24 μm in wild-type to 22 μm in *dyn-1* mutants (**Figure 4C**). The
628 average fiber length was dramatically shorter in the *fzo-1* and *unc-116* mutants, correlating
629 with the presence of larger gaps within degenerating muscle cells in these animals (**Figure
630 2C,E** and **Figure 4C**). These results are consistent with our recent findings studying the effects
631 of mutating CMT2-asscoiated genes in *C. elegans*[20]. Moreover, they highlight the more
632 precise assessment of muscle morphology using these quantitative methods compared to
633 visual scoring alone, and provide evidence that *fzo-1* and *unc-116* are required for normal
634 muscle morphology.
635
636 **Quantitative measurements of mitochondrial morphology using SQUASSH object**
637 **segmentation**
638 To understand how the absence of mitochondrial fission affects mitochondrial morphology in
639 *C. elegans* neurons, we performed quantitative analyses in the PLM mechanosensory
640 neurons. DRP-1, the *C. elegans* orthologue of the mammalian Dynamin-related protein 1
641 (DRP1), controls mitochondrial fission, where upon activation is recruited from the cytosol to
642 form a spiral around mitochondria, constricting and eventually severing both the inner and
643 outer mitochondrial membranes[21,22]. We fluorescently labeled mitochondria with a tissue
644 specific transgene in the PLM neurons, which have a long axonal process that can be readily
645 visualised using epifluorescence microscopy. A loss of fission is hypothesized to disrupt overall
646 mitochondrial dynamics, and therefore decrease the creation of newer, smaller mitochondria
647 through a process known as budding[23].
648
649 We performed SQUASSH segmentation to compare mitochondrial morphology in wild-type
650 and *drp-1* mutant animals. We analyzed the mitochondria from 6 PLM neurons per genotype,
651 resulting in an *n* value of greater that 200 mitochondria for each. Schematic and
652 representative images are shown in **Figure 5A,B**. We found that mutants lacking DRP-1 had
653 larger and more elongated mitochondria (**Figure 5B-F**). Mitochondria in the *drp-1* mutant
654 background were 32% larger than wild-type (*P* = 0.0006, **Figure 5C**), and 14% more elongated

655 (further from a perfect circle) (P < 0.0001, **Figure 5D**). For a more detailed assessment of the
656 variance in size and shape, we plotted histograms for each measure, fitting the data to
657 Gaussian distributions (**Figure 5E,F**). We found that for both size and circularity, mutants
658 lacking the fission protein had a larger variance (p < 0.0001 for both), highlighted by the
659 presence of larger and more elongated mitochondria/mitochondrial networks (see **Figure 5Bii**
660 for examples). Overall, we found evidence to suggest that mutation of *drp-1* causes a lack of
661 fission within PLM neurons, resulting in larger and more elongated mitochondria. We also
662 demonstrated that disruption of mitochondrial fission causes an increase in the variance of
663 mitochondrial morphology.
664
665 **FIGURE LEGENDS:**
666 **Figure 1: Quantification of synapse integrity in the PLM neurons. (A)** Images are maximum
667 z-projections of the PLM synaptic region in a non-transgenic animal. The left panel shows the
668 PLM neuron labelled with tagRFP, the second panel displays the pre-synaptic region labelled
669 with SNB-1::GFP, the third image is an overlay with co-localization represented in yellow, and
670 the fourth panel is a schematic of the overlay image. **(B)** Maximum z-projection confocal
671 images of the synaptic region in animals overexpressing MEC-17. Images are displayed as per
672 panel A. **(C)** Size quantification of the pre-synaptic region in non-transgenic compared to
673 transgenic animals overexpressing MEC-17. **(D)** Quantification of the relative integrated
674 fluorescence levels of SNB-1::GFP in non-transgenics versus transgenic animals
675 overexpressing MEC-17. For (C) and (D), Individual synapses analyzed are represented by
676 circles; $n \geq 10$; mean ± S.E. shown in black. P values * < 0.05, ** < 0.01 from unpaired t-tests;
677 scale bars represent 2 μm.
678
679 **Figure 2: Visualization of the *C. elegans* body wall muscles**. **(A)** An animal expressing the
680 *stEx30(Pmyo-3::gfp::myo-3 + rol-6(su1006))* transgene, which labels myosin heavy chain with
681 GFP in the body wall muscles. The array also induces a rolling phenotype in the animal that
682 facilitates visualization of the muscle cells arranged along the dorsal and ventral sides of the
683 body. Representative magnified views of myosin fibers in **(B)** wild-type, **(C)** *fzo-1(cjn020)*, **(D)**
684 *dyn-1(ky51)* and **(E)** *unc-116(e2310)* animals. All animals were imaged at the 3-day old adult
685 stage. Scale bar represents 60 μm in (A), and 30 μm in (B-E).
686
687 **Figure 3: Measuring body wall muscle area and fiber length using available computational
688 algorithms**. **(A)** Example image demonstrating how the internal gap space within a single
689 muscle cell (red-enclosed), and the area of the entire cell (yellow-enclosed) are drawn and
690 calculated in Fiji to obtain the muscle area ratio. **(B)** Outline of segmentation protocol on a
691 single example image using a combination of Fiji and ilastik. Scale bar represents 30 μm.
692
693 **Figure 4: Qualification and quantification of body wall muscle defects**. **(A)** Visual assessment
694 of body wall muscle defects. **(B)** Comparison of blank space area to total muscle cell area ratio
695 between WT and indicated mutants. **(C)** Measurement of myosin fiber length. For (B) and (C),
696 only images with at least one complete visible oblique muscle cell were included for analysis.
697 Fibers with length of 0 μm or longer than 250 μm were also excluded. Bars represent
698 percentage defective animals in (A) and mean ± S.E.M. in (B) and (C); n values listed in each
699 bar. Chi-square test with false discovery rate were performed to compare visual defects in
700 (A), whereas one-way ANOVA with Dunnett's post hoc tests for multiple comparison were

701 used to analyze quantitative measurements in (B) and (C). *$P < 0.05$, ****$P < 0.0001$, *ns* = not
702 significant.

703

704 **Figure 5: Mitochondrial morphology within the axons of the PLM neurons. (A)** Schematic of
705 a posterior lateral microtubule (PLM) mechanosensory neuron in the tail of *C. elegans*. The
706 red box indicates the approximate location of the highlighted sections in **(B)**, which show
707 representative images of GFP labelled mitochondria (*Pmec-4::MLS::GFP*) within the PLM
708 axon. Bright green puncta indicate mitochondria. Compared to the WT (**i**), *drp-1(tm1108)*
709 mutants (**ii**) show larger, more elongated mitochondria. Images are representative of *n* = 6
710 PLM axons from 6 worms per genotype; scale bars = 15 µm. **(C)** Mean size ($µm^2$) of individual
711 mitochondrion as quantified by SQUASSH object segmentation in 3-day old adult (3DOA)
712 worms. **(D)** Mean Circularity of individual mitochondrion within the PLM axon, as quantified
713 from SQUASSH object measurements in 3DOAs. **(E)** Histogram and Gaussian distribution
714 showing the variance of mitochondrial size. F test ($P < 0.0001$) shows that variances are
715 significantly different between *drp-1* and WT. **(F)** Histogram and Gaussian distribution
716 showing the variance of mitochondrial circularity. Data is represented as mean +/- SEM. ***
717 *$P < 0.001$, **** *$P < 0.0001$ from Welch's t-test; *n* ≥ 204 mitochondria for quantitative analysis
718 from *n* = 6 worms.

719

720 **Table 1. List of *C. elegans* strains used in this study.**

721

722 **Table 2. SQUASSH parameters for segmentation of mitochondria.**

723

724 **DISCUSSION:**
725 Morphological variations have frequently been assessed via manual counting of noticeable
726 differences or using arbitrary thresholds to determine defects in comparison to a wild-type
727 phenotype. More recently, however, quantitative methods have been used for comparative
728 studies of morphology to accurately measure and describe changes on a cellular and
729 subcellular level in an unbiased fashion. The ability to identify subtle yet biologically relevant
730 differences between phenotypes is a powerful means for understanding the underlying
731 molecular mechanisms that control changes in morphology caused by environmental factors
732 or genetic diseases. The continued increases in computation power and microscopy imaging
733 resolution, coupled with the ease of growth and the versatility of *C. elegans* genetics has
734 provided the perfect platform for the combination of sophisticated yet free imaging software
735 with fine detailed confocal images. Here, we have demonstrated methods to evaluate and
736 quantify synaptic size and protein localization, body wall muscle area and fiber length, and
737 mitochondrial morphology in a range of genetic backgrounds.

738

739 While these analyses have demonstrated an ability to quantify subtle morphological
740 differences, there are limitations. Although each of these analyses make use of open-source
741 and readily available software, they rely on high quality, sharp images to accurately resolve
742 cellular structures and subcellular organelles. This can often be a limiting step, as sensitive
743 high-end equipment, such as confocal microscopes with advanced detectors, are required to
744 capture images with satisfactory resolution. These are not always accessible to laboratories,
745 and analysis with sub-par technology can lead to inaccurate and unrepeatable results. In
746 addition, while each technique aims to reduce experimenter bias by using computer
747 algorithms, there are still steps that can involve an element of human error. The manual

definition of the synapse by hand, the outlining of the muscle cell area, the parameter optimizations of mitochondrial segmentation by eye are all areas that can be improved in this respect. To reduce the chance for human error, studies could be conducted in a blinded fashion or alternatively image analysis software could be used to define the region of interest itself. Using cell masks, in which the desired area for analysis is defined by the fluorescence at a different wavelength, may help this. This is used to limit the analysis to a section of an image displaying fluorescence above a set threshold, such as a cell's nucleus or a transfected cell[13,24]. Furthermore, the use of single time point images limits the questions these techniques can address. The processes that govern organelle morphology, synapse formation and muscle structure are most likely dynamic, and differences can be seen within the same cell depending on the developmental or biological status. Analysis of these structures at a specific end-point can therefore be limiting and time-lapse imaging would be beneficial for monitoring structural changes over time. Finally, while morphological changes can be a good indicator of disruption in cellular processes, correlation is not always implicit. For example, recent findings in different species have shown that mitochondrial function and form can indeed be dissociated[7,25]. Therefore, additional assays must be taken into account when inferring functional changes as the result of morphological differences.

We have been able to demonstrate the use of these quantitative techniques in a particular set of tissues and genetic backgrounds; however, their usage can be applied more broadly. Fluorescence quantification via imaging software can be used to analyze a range of different subcellular organelles such as nuclei and endosomes, or different structures such as neurons and epithelial cells, all within the context of different mutant or disease backgrounds.

DISCLOSURES:
The authors declare that they have no competing interests.

REFERENCES:
1   Brenner, S. The genetics of *Caenorhabditis elegans*. *Genetics.* (1974).
2   Markaki, M. & Tavernarakis, N. Modeling human diseases in *Caenorhabditis elegans*. *Biotechnology Journal.* **5** (12), 1261-1276, doi:10.1002/biot.201000183 (2010).
3   Laranjeiro, R., Harinath, G., Burke, D., Braeckman, B.P., & Driscoll, M. Single swim sessions in *C. elegans* induce key features of mammalian exercise. *BMC Biology.* doi:10.1186/s12915-017-0368-4 (2017).
4   Alexander, A.G., Marfil, V., & Li, C. Use of *C. elegans* as a model to study Alzheimer's disease and other neurodegenerative diseases. *Frontiers in Genetics.* doi:10.3389/fgene.2014.00279 (2014).

793   5   Zheng, C., Jin, F.Q., & Chalfie, M. Hox Proteins Act as Transcriptional Guarantors to
794 Ensure Terminal Differentiation. *Cell Reports.* **13** (7), 1343-1352,
795 doi:10.1016/j.celrep.2015.10.044 (2015).

796 6   Koushika, S.P. *et al.* Mutations in *Caenorhabditis elegans* cytoplasmic dynein
797 components reveal specificity of neuronal retrograde cargo. *Journal of Neuroscience.* **24** (16),
798 3907-3916, doi:10.1523/JNEUROSCI.5039-03.2004 (2004).

799 7   Byrne, J.J. *et al.* Disruption of mitochondrial dynamics affects behaviour and lifespan
800 in *Caenorhabditis elegans*. *Cellular and Molecular Life Sciences.* doi:10.1007/s00018-019-
801 03024-5 (2019).

802 8   Campagnola, P.J. *et al.* Three-Dimensional High-Resolution Second-Harmonic
803 Generation Imaging of Endogenous Structural Proteins in Biological Tissues. *Biophysical
804 Journal.* **82** (1), 493-508, doi:10.1016/S0006-3495(02)75414-3 (2002).

805 9   Schindelin, J. *et al.* Fiji: An open-source platform for biological-image analysis. *Nature
806 Methods*. **9** (7), 676-82, doi: 10.1038/nmeth.2019 (2012).

807 10   Sommer, C., Straehle, C., Kothe, U., & Hamprecht, F.A. Ilastik: Interactive learning and
808 segmentation toolkit. *2011 IEEE International Symposium on Biomedical Imaging: From Nano
809 to Macro*, doi: 10.1109/ISBI.2011.5872394 (2011).

810 11   Mondal, S., Ahlawat, S., & Koushika, S.P. Simple microfluidic devices for *in vivo* imaging
811 of *C. elegans*, *Drosophila* and zebrafish. *Journal of Visualized Experiments.* doi:10.3791/3780
812 (2012).

813 12   Paul, G., Cardinale, J., & Sbalzarini, I.F. Coupling image restoration and segmentation:
814 A generalized linear model/bregman perspective. *International Journal of Computer Vision.*
815 doi:10.1007/s11263-013-0615-2 (2013).

816 13   Rizk, A. *et al.* Segmentation and quantification of subcellular structures in fluorescence
817 microscopy images using Squassh. *Nature Protocols.* **9**, 586-586 (2014).

818 14   Akella, J.S. *et al.* MEC-17 is an alpha-tubulin acetyltransferase. *Nature.* **467** (7312),
819 218-222, doi:10.1038/nature09324 (2010).

820 15   Neumann, B. & Hilliard, M.A. Loss of MEC-17 leads to microtubule instability and
821 axonal degeneration. *Cell Reports.* **6** (1), 93-103, doi:10.1016/j.celrep.2013.12.004 (2014).

822 16   Shida, T., Cueva, J.G., Xu, Z., Goodman, M.B., & Nachury, M.V. The major alpha-tubulin
823 K40 acetyltransferase alphaTAT1 promotes rapid ciliogenesis and efficient
824 mechanosensation. *Proceedings of the National Academy of Sciences of the United States of
825 America.* **107** (50), 21517-21522, doi:10.1073/pnas.1013728107 (2010).

826 17   Teoh, J.-S., Wang, W., Chandhok, G., Pocock, R., & Neumann, B. Development and
827 maintenance of synaptic structure is mediated by the alpha-tubulin acetyltransferase MEC-
828 17/αTAT1. *bioRxiv.* **84**, 522904-522904, doi:10.1101/522904 (2019).

829 18   Bird, T.D. *Charcot-Marie-Tooth Neuropathy Type 2.* GeneReviews [Internet]. Seattle
830 (WA): University of Washington, Seattle; 1993-2019. [Updated 2016 Apr 14] Available from:
831 https://www.ncbi.nlm.nih.gov/books/NBK1285/ (1998).

832 19   Chandhok, G., Lazarou, M., & Neumann, B. Structure, function, and regulation of
833 mitofusin-2 in health and disease. *Biological Reviews.* **93** (2), 933-949, doi:10.1111/brv.12378
834 (2018).

835 20   Soh, M.S., Cheng, X., Liu, J., & Neumann, B. Disruption of genes associated with
836 Charcot-Marie-Tooth type 2 lead to common behavioural, cellular and molecular defects in
837 *Caenorhabditis elegans*. *bioRxiv.* 605584, doi:10.1101/605584 (2019).

838   21   Kamerkar, S.C., Kraus, F., Sharpe, A.J., Pucadyil, T.J., & Ryan, M.T. Dynamin-related
839 protein 1 has membrane constricting and severing abilities sufficient for mitochondrial and
840 peroxisomal fission. *Nature Communications.* doi:10.1038/s41467-018-07543-w (2018).

841   22   Zhu, P.-P. *et al.* Intra- and Intermolecular Domain Interactions of the C-terminal
842 GTPase Effector Domain of the Multimeric Dynamin-like GTPase Drp1. *Journal of Biological*
843 *Chemistry.* **279** (34), 35967-35974, doi:10.1074/JBC.M404105200 (2004).

844   23   Osellame, L.D. *et al.* Cooperative and independent roles of the Drp1 adaptors Mff,
845 MiD49 and MiD51 in mitochondrial fission. *Journal of Cell Science.* doi:10.1242/jcs.185165
846 (2016).

847   24   Dima, A.A. *et al.* Comparison of segmentation algorithms for fluorescence microscopy
848 images of cells. *Cytometry Part A.* **79A** (7), 545-559, doi:10.1002/cyto.a.21079 (2011).

849   25   Trevisan, T. *et al.* Manipulation of Mitochondria Dynamics Reveals Separate Roles for
850 Form and Function in Mitochondria Distribution. *Cell Reports.*
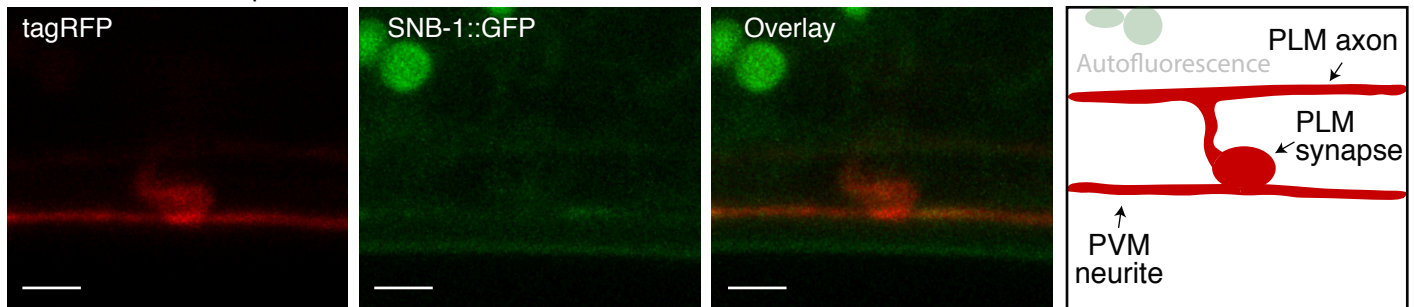851 doi:10.1016/j.celrep.2018.04.017 (2018).

852
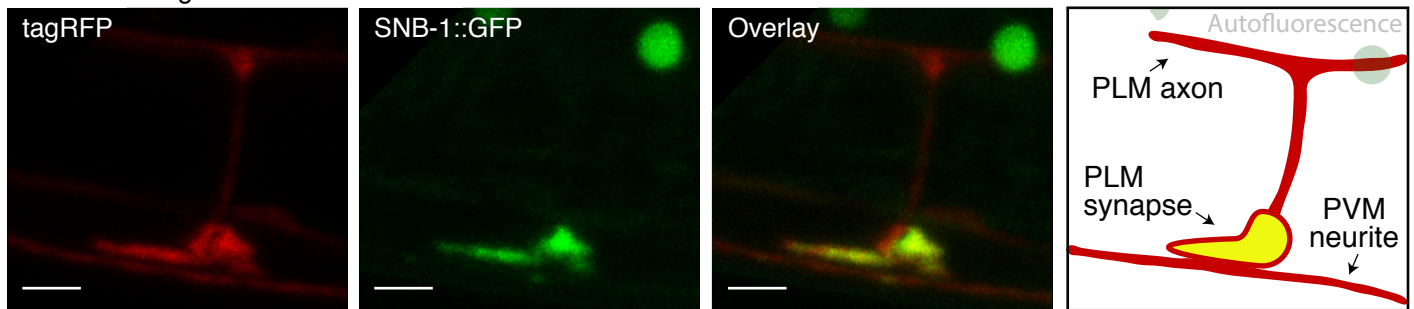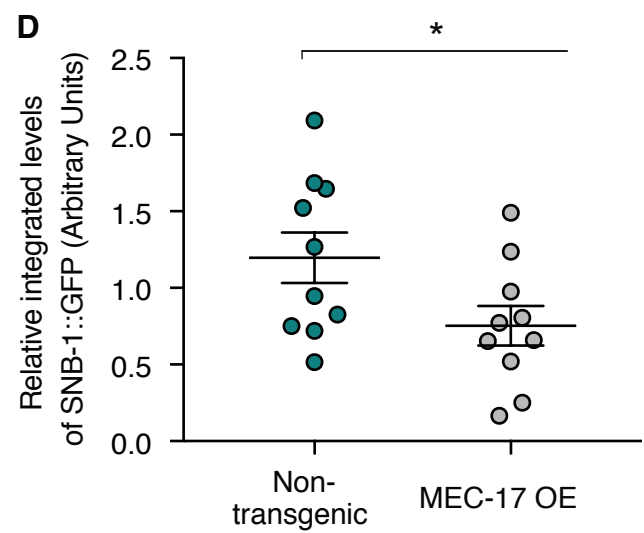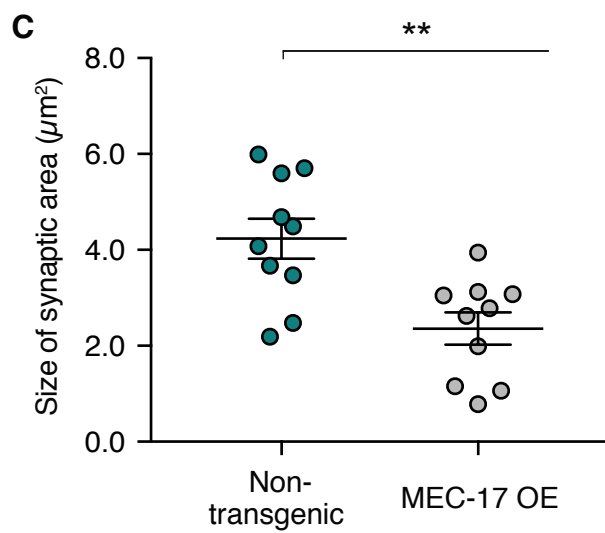
Figure 1

Figure 2

Figure 2

A wild-type

GFP::MYO-3

Anterior

Posterior
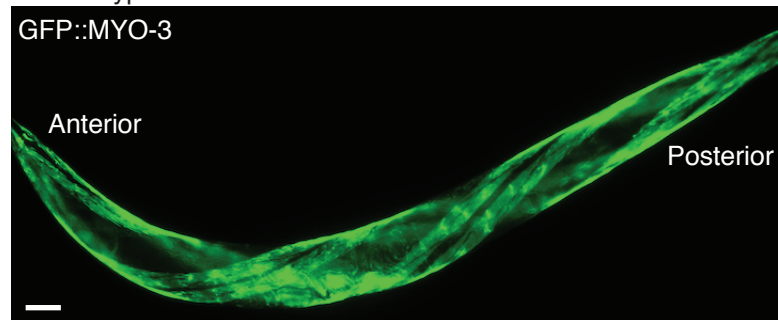
B wild-type
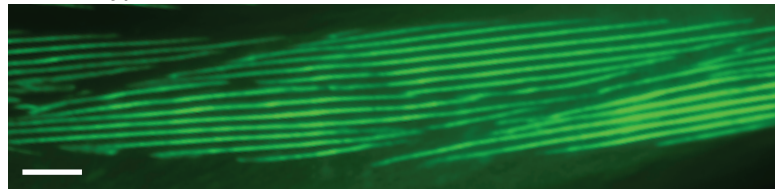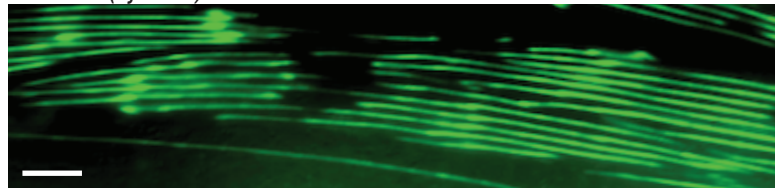
C *fzo-1(cjn020)*

D *dyn-1(ky51)*
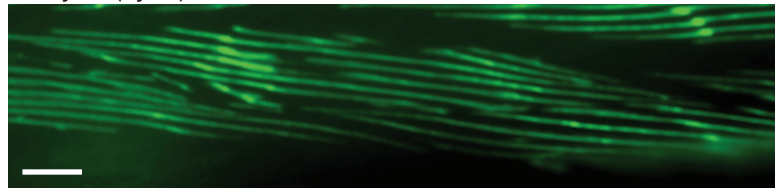
E *unc-116(e2310)*

Figure 3

Figure 3

A

GFP::MYO-3

muscle area ratio = $\dfrac{\text{gap within single cell}}{\text{total single cell area}}$

B

Original image of a muscle cell

↓

Classification and segregation of muscle fibres from background using Ilastik

↓

Conversion of individual fibres to 'skeletons' that can then be analysed in Fiji

Figure 4

Figure 4

A Visual assessment

B Muscle area quantification

C Myosin fibre length measurement

Figure 5

Figure 5

Table 1
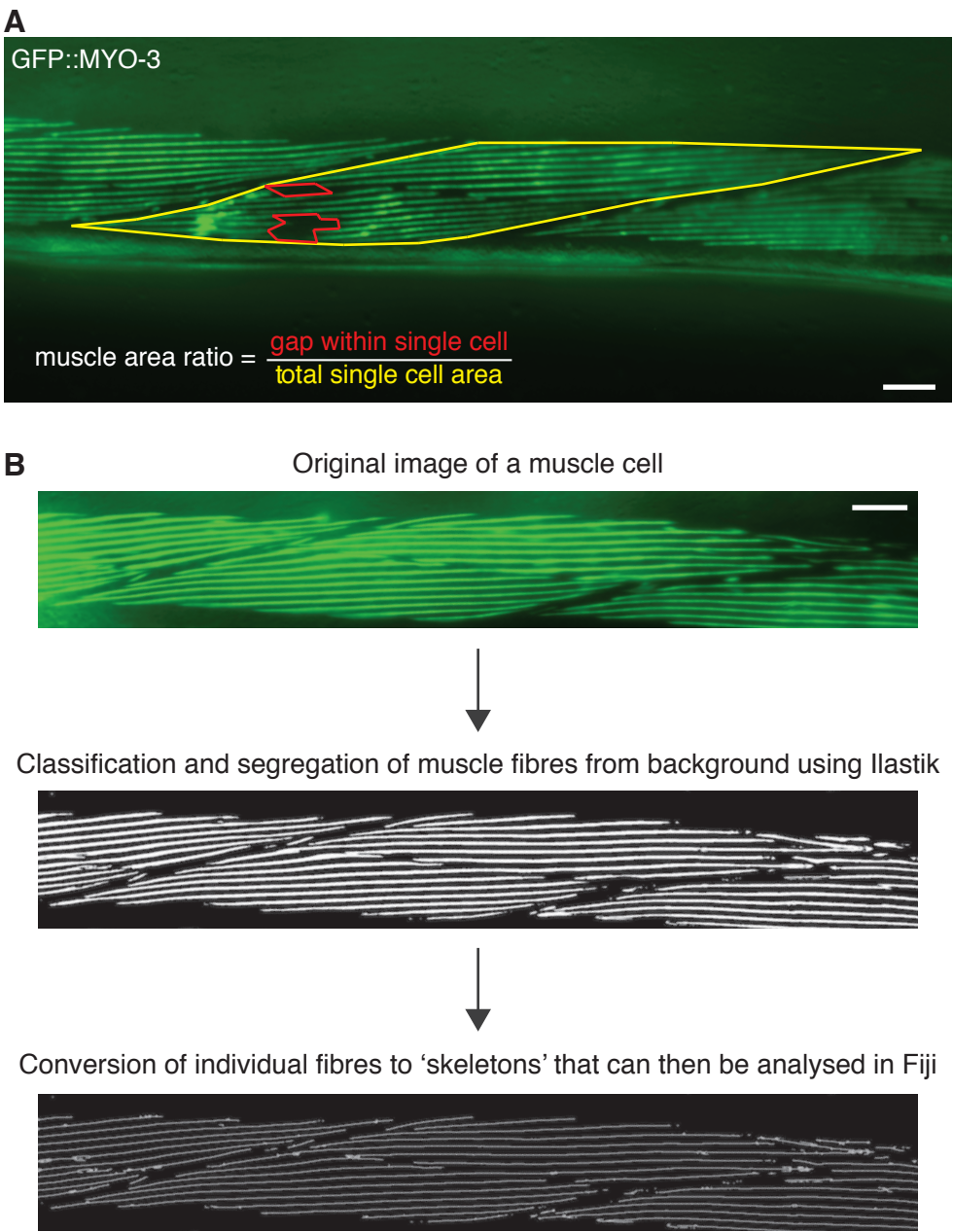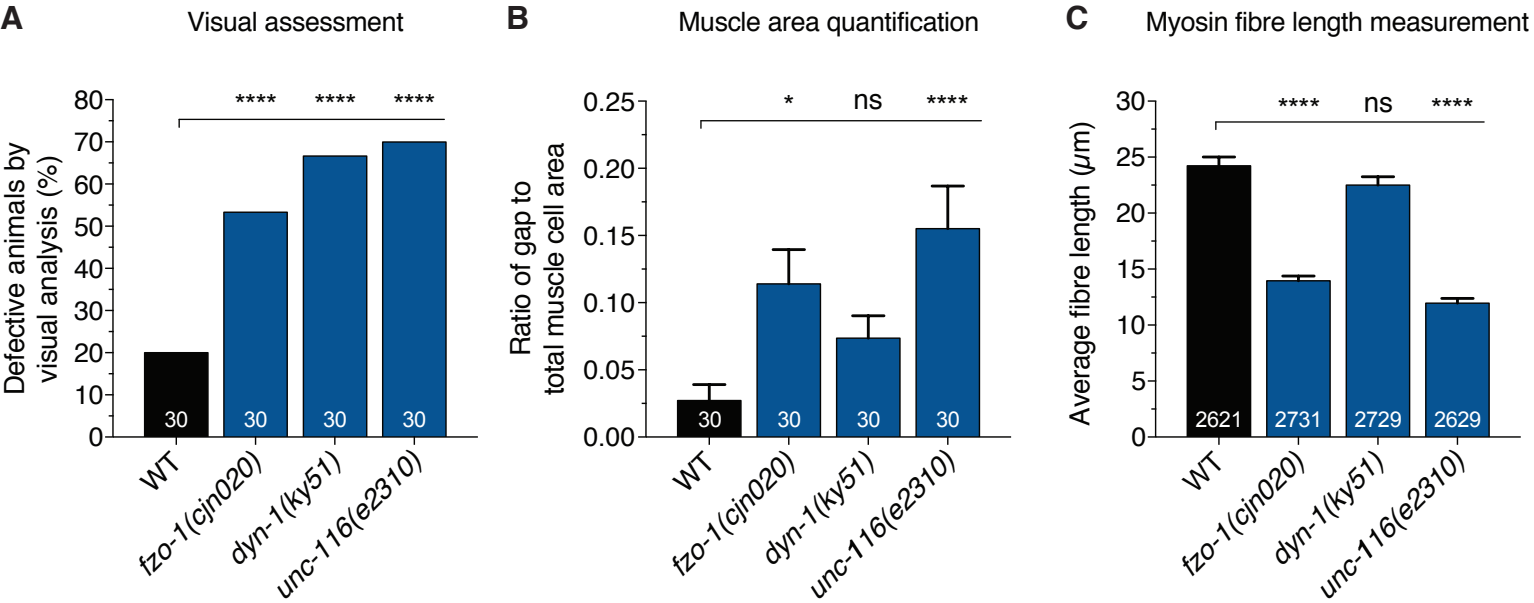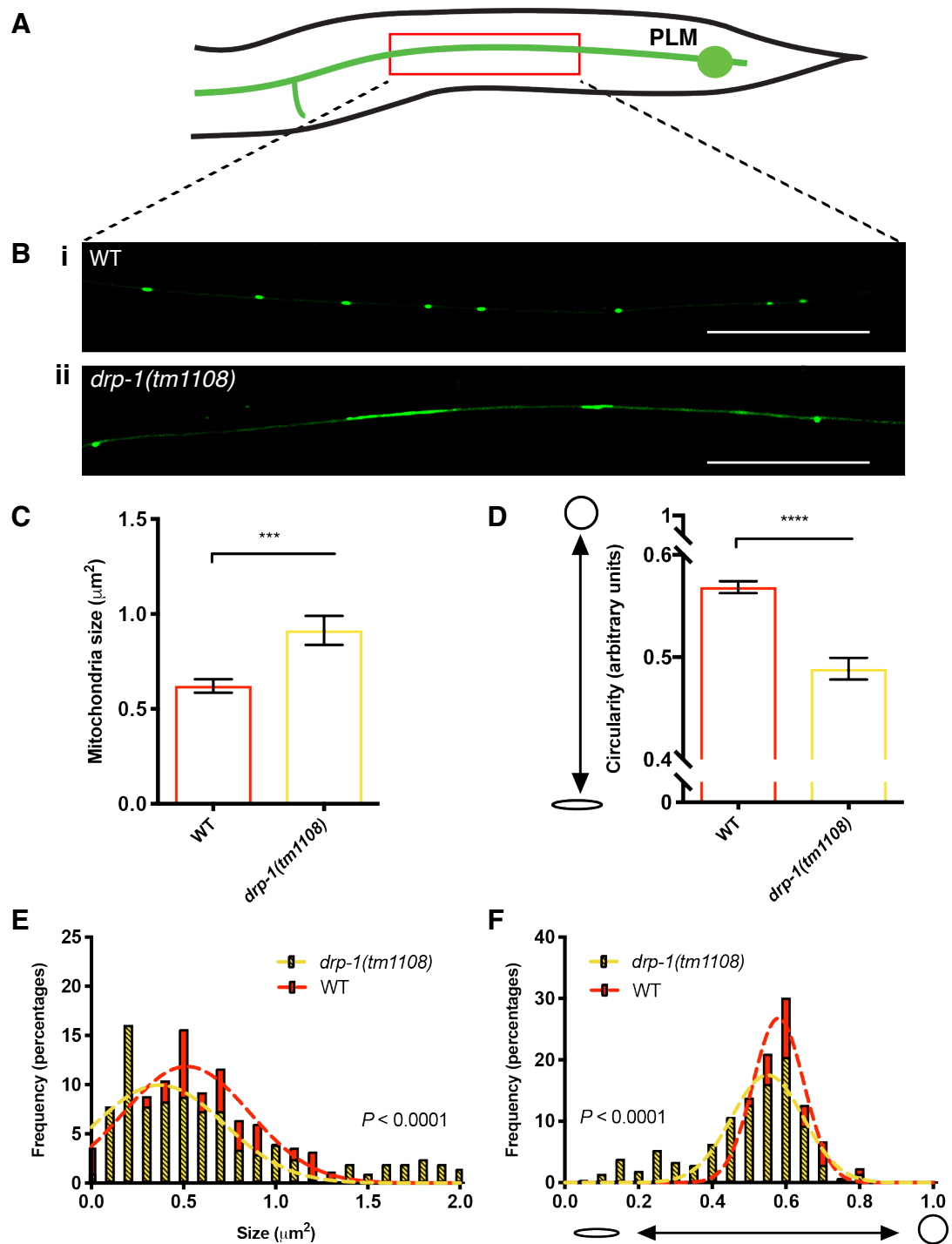
Table 1. List o

Strain name
BXN038
BXN366
BXN419
BXN507
BXN675
BXN685
NM664
RW1596
TU4065

of *C. elegans* strains used in this study

Genotype

uIs115(Pmec-17::tagRFP); jsIs609(Pmec-4::MLS::GFP)

fzo-1(cjn020); myo-3(st386); zdIs5(Pmec-4::GFP); stEx30(Pmyo-3::gfp::myo-3 + rol-6(su1006))

drp-1(tm1108); jsIs609(Pmec-4::MLS::GFP); uIs115(Pmec-17::tagRFP)

cjnEx036(Pmec-4::mec-17, Pmyo-2::mCherry); jsIs37(Pmec-7::snb-1::GFP); lin-15B&lin-15A(n765); uIs115

unc-116(e2310); myo-3(st386); stEx30(Pmyo-3::gfp::myo-3 + rol-6(su1006))

dyn-1(ky51); myo-3(st386); stEx30(Pmyo-3::gfp::myo-3 + rol-6(su1006))

jsIs37(Pmec-7::snb-1::GFP); lin-15B&lin-15A(n765)

myo-3(st386); stEx30(Pmyo-3::gfp::myo-3 + rol-6(su1006))

uIs115(Pmec-17::tagRFP)

Source	Reference #
Neumann lab	7
Neumann lab	20
Neumann lab	7
Neumann lab	17
Neumann lab	20
Neumann lab	20
Caenorhabditis Genetics Center	6
Caenorhabditis Genetics Center	8
Martin Chalfie	5

	PLM axon images
Objective	40x
Image resolution (per panel for tilescan)	3224 x 3224
Background removal window size	20
PSF xy	0.78
PSF z	0.68
Regularisation	0.15
Minimum fluorescence intensity of GFP	0.4

Name of Material/Equipment	Company	Catalog Number	Comments/Description
Agar-agar	Merck	1.01614.1000	
Agarose	Invitrogen	16500-500	
Confocal microscope	Leica	TCS SP8	Inverted platform
Fluorescence microscope	Carl Zeiss AG	Zeiss Axio Imager M2	
Glass coverslips #1	Thermo scientifique	MENCS22221GP	
Glass coverslips #1.5	Zeiss	474030-9000-000	Made by SCHOTT
Glass slides	Thermo scientifique	MENS41104A/40	
Light LED	Schott	KL 300 LED	
Stereo Microscope	Olympus	SZ51	
Tryptone (Peptone from casein)	Merck	107213	Ingredients for Lysogeny
Yeast Extract	Merck	103753	Broth (LB) medium
Sodium chloride	Merck	106404	
Peptone (Peptone from meat)	Merck	107214	
Agar	Sigma	A1296	
Sodium chloride	Merck	106404	Ingredients for Nematode
Cholesterol	Sigma	C8667-25G	Growth Media (NGM)
Calcium chloride	Merck	102382	agar
Magnesium sulfate	Merck	105886	
Dipotassium phosphate	Merck	105101	
Potassium dihydrogen phosphate	Merck	104873	
Disodium phosphate	Merck	106586	
Sodium chloride	Merck	106404	
			Ingredients for M9 buffer
Potassium dihydrogen phosphate	Merck	104873	

Magnesium sulfate	Merck	105886
Pasteur pipette	Corning	CLS7095D5X-200EA
Petri dishes	Corning	CLS430589-500EA
Platinum wire	Sigma	267201-2G
Spatula	Met-app	2616
Tetramisole hydrochloride	Sigma	L9756-5G

jove
JOURNAL OF VISUALIZED EXPERIMENTS

1 Alewife Center #200
Cambridge, MA 02140
tel. 617.945.9051
www.jove.com

ARTICLE AND VIDEO LICENSE AGREEMENT

Title of Article:	Quantitative approaches for studying cellular structures and organelle morphology in *C. elegans*
Author(s):	Jean-Sébastien Teoh, Ming S. Soh, Joseph J. Byrne, Brent Neumann

Item 1: The Author elects to have the Materials be made available (as described at http://www.jove.com/publish) via:

[X] Standard Access   [ ] Open Access

Item 2: Please select one of the following items:

[X] The Author is **NOT** a United States government employee.

[ ] The Author is a United States government employee and the Materials were prepared in the course of his or her duties as a United States government employee.

[ ] The Author is a United States government employee but the Materials were NOT prepared in the course of his or her duties as a United States government employee.

ARTICLE AND VIDEO LICENSE AGREEMENT

1.   **Defined Terms.** As used in this Article and Video License Agreement, the following terms shall have the following meanings: "**Agreement**" means this Article and Video License Agreement; "**Article**" means the article specified on the last page of this Agreement, including any associated materials such as texts, figures, tables, artwork, abstracts, or summaries contained therein; "**Author**" means the author who is a signatory to this Agreement; "**Collective Work**" means a work, such as a periodical issue, anthology or encyclopedia, in which the Materials in their entirety in unmodified form, along with a number of other contributions, constituting separate and independent works in themselves, are assembled into a collective whole; "**CRC License**" means the Creative Commons Attribution-Non Commercial-No Derivs 3.0 Unported Agreement, the terms and conditions of which can be found at: http://creativecommons.org/licenses/by-nc-nd/3.0/legalcode; "**Derivative Work**" means a work based upon the Materials or upon the Materials and other pre-existing works, such as a translation, musical arrangement, dramatization, fictionalization, motion picture version, sound recording, art reproduction, abridgment, condensation, or any other form in which the Materials may be recast, transformed, or adapted; "**Institution**" means the institution, listed on the last page of this Agreement, by which the Author was employed at the time of the creation of the Materials; "**JoVE**" means MyJove Corporation, a Massachusetts corporation and the publisher of The Journal of Visualized Experiments; "**Materials**" means the Article and / or the Video; "**Parties**" means the Author and JoVE; "**Video**" means any video(s) made by the Author, alone or in conjunction with any other parties, or by JoVE or its affiliates or agents, individually or in collaboration with the Author or any other parties, incorporating all or any portion

of the Article, and in which the Author may or may not appear.

2.   **Background.** The Author, who is the author of the Article, in order to ensure the dissemination and protection of the Article, desires to have the JoVE publish the Article and create and transmit videos based on the Article. In furtherance of such goals, the Parties desire to memorialize in this Agreement the respective rights of each Party in and to the Article and the Video.

3.   **Grant of Rights in Article.** In consideration of JoVE agreeing to publish the Article, the Author hereby grants to JoVE, subject to **Sections 4** and **7** below, the exclusive, royalty-free, perpetual (for the full term of copyright in the Article, including any extensions thereto) license (a) to publish, reproduce, distribute, display and store the Article in all forms, formats and media whether now known or hereafter developed (including without limitation in print, digital and electronic form) throughout the world, (b) to translate the Article into other languages, create adaptations, summaries or extracts of the Article or other Derivative Works (including, without limitation, the Video) or Collective Works based on all or any portion of the Article and exercise all of the rights set forth in (a) above in such translations, adaptations, summaries, extracts, Derivative Works or Collective Works and (c) to license others to do any or all of the above. The foregoing rights may be exercised in all media and formats, whether now known or hereafter devised, and include the right to make such modifications as are technically necessary to exercise the rights in other media and formats. If the "Open Access" box has been checked in **Item 1** above, JoVE and the Author hereby grant to the public all such rights in the Article as provided in, but subject to all limitations and requirements set forth in, the CRC License.

612542.6   For questions, please contact us at submissions@jove.com or +1.617.945.9051.

![jove logo] 1 Alewife Center #200
Cambridge, MA 02140
tel. 617.945.9051
www.jove.com

ARTICLE AND VIDEO LICENSE AGREEMENT

4.   **Retention of Rights in Article.** Notwithstanding the exclusive license granted to JoVE in **Section 3** above, the Author shall, with respect to the Article, retain the non-exclusive right to use all or part of the Article for the non-commercial purpose of giving lectures, presentations or teaching classes, and to post a copy of the Article on the Institution's website or the Author's personal website, in each case provided that a link to the Article on the JoVE website is provided and notice of JoVE's copyright in the Article is included. All non-copyright intellectual property rights in and to the Article, such as patent rights, shall remain with the Author.

5.   **Grant of Rights in Video – Standard Access.** This **Section 5** applies if the "Standard Access" box has been checked in **Item 1** above or if no box has been checked in **Item 1** above. In consideration of JoVE agreeing to produce, display or otherwise assist with the Video, the Author hereby acknowledges and agrees that, Subject to **Section 7** below, JoVE is and shall be the sole and exclusive owner of all rights of any nature, including, without limitation, all copyrights, in and to the Video. To the extent that, by law, the Author is deemed, now or at any time in the future, to have any rights of any nature in or to the Video, the Author hereby disclaims all such rights and transfers all such rights to JoVE.

6.   **Grant of Rights in Video – Open Access.** This **Section 6** applies only if the "Open Access" box has been checked in **Item 1** above. In consideration of JoVE agreeing to produce, display or otherwise assist with the Video, the Author hereby grants to JoVE, subject to **Section 7** below, the exclusive, royalty-free, perpetual (for the full term of copyright in the Article, including any extensions thereto) license (a) to publish, reproduce, distribute, display and store the Video in all forms, formats and media whether now known or hereafter developed (including without limitation in print, digital and electronic form) throughout the world, (b) to translate the Video into other languages, create adaptations, summaries or extracts of the Video or other Derivative Works or Collective Works based on all or any portion of the Video and exercise all of the rights set forth in (a) above in such translations, adaptations, summaries, extracts, Derivative Works or Collective Works and (c) to license others to do any or all of the above. The foregoing rights may be exercised in all media and formats, whether now known or hereafter devised, and include the right to make such modifications as are technically necessary to exercise the rights in other media and formats. For any Video to which this **Section 6** is applicable, JoVE and the Author hereby grant to the public all such rights in the Video as provided in, but subject to all limitations and requirements set forth in, the CRC License.

7.   **Government Employees.** If the Author is a United States government employee and the Article was prepared in the course of his or her duties as a United States government employee, as indicated in **Item 2** above, and any of the licenses or grants granted by the Author hereunder exceed the scope of the 17 U.S.C. 403, then the rights granted hereunder shall be limited to the maximum

rights permitted under such statute. In such case, all provisions contained herein that are not in conflict with such statute shall remain in full force and effect, and all provisions contained herein that do so conflict shall be deemed to be amended so as to provide to JoVE the maximum rights permissible within such statute.

8.   **Protection of the Work.** The Author(s) authorize JoVE to take steps in the Author(s) name and on their behalf if JoVE believes some third party could be infringing or might infringe the copyright of either the Author's Article and/or Video.

9.   **Likeness, Privacy, Personality.** The Author hereby grants JoVE the right to use the Author's name, voice, likeness, picture, photograph, image, biography and performance in any way, commercial or otherwise, in connection with the Materials and the sale, promotion and distribution thereof. The Author hereby waives any and all rights he or she may have, relating to his or her appearance in the Video or otherwise relating to the Materials, under all applicable privacy, likeness, personality or similar laws.

10.   **Author Warranties.** The Author represents and warrants that the Article is original, that it has not been published, that the copyright interest is owned by the Author (or, if more than one author is listed at the beginning of this Agreement, by such authors collectively) and has not been assigned, licensed, or otherwise transferred to any other party. The Author represents and warrants that the author(s) listed at the top of this Agreement are the only authors of the Materials. If more than one author is listed at the top of this Agreement and if any such author has not entered into a separate Article and Video License Agreement with JoVE relating to the Materials, the Author represents and warrants that the Author has been authorized by each of the other such authors to execute this Agreement on his or her behalf and to bind him or her with respect to the terms of this Agreement as if each of them had been a party hereto as an Author. The Author warrants that the use, reproduction, distribution, public or private performance or display, and/or modification of all or any portion of the Materials does not and will not violate, infringe and/or misappropriate the patent, trademark, intellectual property or other rights of any third party. The Author represents and warrants that it has and will continue to comply with all government, institutional and other regulations, including, without limitation all institutional, laboratory, hospital, ethical, human and animal treatment, privacy, and all other rules, regulations, laws, procedures or guidelines, applicable to the Materials, and that all research involving human and animal subjects has been approved by the Author's relevant institutional review board.

11.   **JoVE Discretion.** If the Author requests the assistance of JoVE in producing the Video in the Author's facility, the Author shall ensure that the presence of JoVE employees, agents or independent contractors is in accordance with the relevant regulations of the Author's institution. If more than one author is listed at the beginning of this Agreement, JoVE may, in its sole

discretion, elect not take any action with respect to the Article until such time as it has received complete, executed Article and Video License Agreements from each such author. JoVE reserves the right, in its absolute and sole discretion and without giving any reason therefore, to accept or decline any work submitted to JoVE. JoVE and its employees, agents and independent contractors shall have full, unfettered access to the facilities of the Author or of the Author's institution as necessary to make the Video, whether actually published or not. JoVE has sole discretion as to the method of making and publishing the Materials, including, without limitation, to all decisions regarding editing, lighting, filming, timing of publication, if any, length, quality, content and the like.

12.   **Indemnification.** The Author agrees to indemnify JoVE and/or its successors and assigns from and against any and all claims, costs, and expenses, including attorney's fees, arising out of any breach of any warranty or other representations contained herein. The Author further agrees to indemnify and hold harmless JoVE from and against any and all claims, costs, and expenses, including attorney's fees, resulting from the breach by the Author of any representation or warranty contained herein or from allegations or instances of violation of intellectual property rights, damage to the Author's or the Author's institution's facilities, fraud, libel, defamation, research, equipment, experiments, property damage, personal injury, violations of institutional, laboratory, hospital, ethical, human and animal treatment, privacy or other rules, regulations, laws, procedures or guidelines, liabilities and other losses or damages related in any way to the submission of work to JoVE, making of videos by JoVE, or publication in JoVE or elsewhere by JoVE. The Author shall be responsible for, and shall hold JoVE harmless from, damages caused by lack of sterilization, lack of cleanliness or by contamination due to

the making of a video by JoVE its employees, agents or independent contractors. All sterilization, cleanliness or decontamination procedures shall be solely the responsibility of the Author and shall be undertaken at the Author's expense. All indemnifications provided herein shall include JoVE's attorney's fees and costs related to said losses or damages. Such indemnification and holding harmless shall include such losses or damages incurred by, or in connection with, acts or omissions of JoVE, its employees, agents or independent contractors.

13.   **Fees.** To cover the cost incurred for publication, JoVE must receive payment before production and publication of the Materials. Payment is due in 21 days of invoice. Should the Materials not be published due to an editorial or production decision, these funds will be returned to the Author. Withdrawal by the Author of any submitted Materials after final peer review approval will result in a US$1,200 fee to cover pre-production expenses incurred by JoVE. If payment is not received by the completion of filming, production and publication of the Materials will be suspended until payment is received.

14.   **Transfer, Governing Law.** This Agreement may be assigned by JoVE and shall inure to the benefits of any of JoVE's successors and assignees. This Agreement shall be governed and construed by the internal laws of the Commonwealth of Massachusetts without giving effect to any conflict of law provision thereunder. This Agreement may be executed in counterparts, each of which shall be deemed an original, but all of which together shall be deemed to me one and the same agreement. A signed copy of this Agreement delivered by facsimile, e-mail or other means of electronic transmission shall be deemed to have the same legal effect as delivery of an original signed copy of this Agreement.

A signed copy of this document must be sent with all new submissions. Only one Agreement is required per submission.

CORRESPONDING AUTHOR

Name:

| Brent Neumann |

Department:

| Biomedicine Discovery Institute |

Institution:

| Monash University |

Title:

| Dr |

Signature: [signature]   Date: 7th March, 2019

Please submit a **signed** and **dated** copy of this license by one of the following three methods:
1. Upload an electronic version on the JoVE submission site
2. Fax the document to +1.866.381.2236
3. Mail the document to JoVE / Attn: JoVE Editorial / 1 Alewife Center #200 / Cambridge, MA 02140

612542.6   For questions, please contact us at submissions@jove.com or +1.617.945.9051.

Brent Neumann, PhD
Group Leader/Senior Research Fellow
Neuroscience Program, Monash Biomedicine Discovery Institute and Department of
Anatomy and Developmental Biology
Monash University
Melbourne VIC 3800, Australia
Ph: +61 3 9905 0670
Email: brent.neumann@monash.edu
http://www.neumannlab.com

16th April 2019

Dear Dr Wu,

We are submitting a revised version of manuscript JoVE59978_R1, entitled "**Quantitative
approaches for studying cellular structures and organelle morphology in *C.
elegans*".

We have addressed the second round of editorial comments and made the appropriate
revisions to our manuscript. All changes have been tracked in the submitted document,
and included here below is a point-by-point response to the each of the comments
received.

We trust that our manuscript will now be suitable for publication in the *Journal of
Visualized Experiments*.

Sincerely,

Brent Neumann

Editorial comments

The manuscript has been modified and the updated manuscript, 59978_R1.docx, is attached and located in your Editorial Manager account. Please use the updated version to make your revisions.

All changes have been made using the modified version.

1. Please take this opportunity to thoroughly proofread the manuscript to ensure that there are no spelling or grammar issues.

We have thoroughly proofread the manuscript again.

2. Please avoid long steps/notes (more than 4 lines).

We have shortened or split our long protocol steps to avoid going beyond 4 lines where possible.

3. JoVE cannot publish manuscripts containing commercial language. This includes company names of an instrument or reagent. Please remove all commercial language from your manuscript and use generic terms instead. All commercial products should be sufficiently referenced in the Table of Materials and Reagents. Examples of commercial language in your manuscript include Leica, Zeiss, HyD, etc.

We have removed all references to commercial products.

4. Step 5.1.2: Please write this step in the imperative tense.

We have revised the tense of this step.

5. 5.3.14: Please write this step in the imperative tense.

We have revised the tense of this step.

6. Please do not abbreviate journal titles for references.

We have revised our reference list.